Supplementary Information

Size-controlled synthesis of ultrasmall Cu_3VS_4 nanocrystals *via* direct ternary nucleation

Zhaohong Sun, Brendan Ward-O'Brien, Yizhen Chen, and Richard L. Brutchey*

Department of Chemistry, University of Southern California, Los Angeles, California 90089, United States. *Email: brutchey@usc.edu

Experimental Section

General Considerations. Copper(I) iodide (CuI, 99.999%, Strem), vanadyl acetylacetonate ($VO(acac)_2$, ≥97.0%, Sigma-Aldrich), carbon disulfide (CS_2, ≥99.9%, Sigma-Aldrich), oleylamine (70%, Sigma-Aldrich), and 1-dodecanethiol (98%, Thermo Scientific) were obtained as indicated. Oleylamine and 1-dodecanethiol were degassed under vacuum at 120 °C for 4 h before use. CS_2 was dried using 4 Å molecular sieves. All syntheses were performed under a nitrogen atmosphere using standard Schlenk techniques. Temperature control and monitoring were carried out using J-KEM controllers equipped with *in-situ* thermocouples.

Size-Controlled Synthesis of Ultrasmall Cu_3VS_4 Nanocrystals. CuI (2.64 mmol, 0.503 g), $VO(acac)_2$ (0.880 mmol, 0.233 g), and oleylamine (22.0 mL) were degassed in a three-neck round-bottom flask at 100 °C for 10 min to yield a 0.04 M [Cu_3V] precursor solution. 5.00 mL of the [Cu_3V] precursor solution (0.200 mmol) was transferred to a clean three-neck round-bottom flask under flowing nitrogen and heated to the target temperature (180, 210, 240, or 270 °C), when CS_2 (2.00 mmol, 0.120 mL) was swiftly injected. The exothermic reaction of CS_2 and oleylamine resulted in a temperature increase of ~15 °C. Due to the gas evolution upon injection, it is advised to use a 25 mL flask for a 5 mL reaction to prevent insufficient reflux. After 5 min, the reaction suspension was thermally quenched by placing it in a room-temperature water bath. The suspension was transferred to a 50 mL centrifuge tube, and the residual product in the flask was washed multiple times with ethanol and added to the centrifuge tube. Finally, ~2 mL of hexanes was used to wash and transfer residual nanocrystals in the flask. The addition of excess hexanes (>5 mL) should be strictly avoided to guarantee nanocrystal precipitation upon centrifugation. The centrifuge tube was then filled to 45 mL with ethanol, sonicated for 3 min, and centrifuged at 6000 rpm for 5 min. The precipitate was resuspended in 45 mL of ethanol, sonicated for 3 min, and centrifuged again at 6000 rpm for 5 min. The nanocrystal precipitates were redispersed in hexanes or dried to a powder for characterization. Appropriate amounts of 1-dodecanethiol were added to the hexanes suspension to achieve long-term colloidal stability.

Aliquot Studies. Reaction aliquots (~1 mL) were withdrawn at designated reaction times using a Hamilton Gastight 1000 Series syringe (purged with nitrogen). Each aliquot was immediately injected into 10 mL of ethanol for quenching, then centrifuged and washed with hexanes/ethanol. Syringe and needle were rinsed with hexanes between samplings to prevent cross-contamination.

Characterization. Powder X-ray diffraction (XRD) measurements were conducted on a Rigaku Miniflex powder X-ray diffractometer using Cu *K*α radiation (λ = 1.541 Å). Powder

samples were prepared on a zero-diffraction silicon substrate. Raman spectroscopy was conducted on powder samples on Si substrates, using a Horiba XploRA confocal Raman microscope with 785 nm excitation. Ultraviolet–visible–near-infrared (UV-vis-NIR) spectra were collected from nanocrystal suspensions dispersed in hexanes in a quartz cuvette, using a Shimadzu UV-1800 UV-vis-NIR spectrometer. Scanning electron microscopy (SEM) was performed on powder samples on carbon tape substrates using an Apreo 2 microscope at an operating voltage of 30 kV, with energy dispersive X-ray spectroscopy (EDX) performed using an Oxford UltimMax 170 silicon drift EDX detector. Standardless semiquantitative analysis of EDX was performed based on factory-calibrated corrections using the AZtec software from Oxford Instruments. Emission lines used for analysis are: *K* series for S, V, and Cu. Factory standards used for quantification are: FeS_2 for S, V for V, and Cu for Cu. A representative raw EDX spectrum of Cu_3VS_4 nanocrystals synthesized at 180 °C is shown in Fig. S2. Transmission electron microscopy (TEM) was performed on dropcast samples supported on carbon-coated copper TEM grids (Ted Pella, Inc.), using an FEI Talos F200C G2 microscope at an operating voltage of 200 kV, equipped with a Ceta complementary metal-oxide-semiconductor (CMOS) camera. Small-angle X-ray scattering (SAXS) patterns were collected using a Xenocs Xeuss 3.0 system equipped with a Dectris EIGER2 R 1M detector and a Cu *K*α X-ray source. Nanocrystal suspensions in hexanes were contained in epoxy-sealed quartz capillaries with 1.5 mm inner diameters (Charles Supper), while the rest of the sample chamber was evacuated to reduce air scattering. The sample-detector distance was calibrated using a silver behenate film, and hexanes was used for background. Data reduction and background subtraction were performed on Xenocs' XSACT software, and fittings were performed using SasView v6.1.[1] The fittings simulate the particles as spheres that have a scattering contrast, $\Delta\rho$, of 2.35×10^{-5} Å^{-2}, assuming a density of 3.81 g/cm^3. X-ray photoelectron spectroscopy (XPS) was performed on powdered samples supported on Ti plates, using an ESCALAB QXi system equipped with a monochromated, micro-focused Al *K*α X-ray source, a bi-polar hemispherical analyzer, and a flood gun for charge compensation. Binding energies were referenced to the C 1s core level at 284.8 eV.

Rietveld Refinement and Scherrer Analysis. Rietveld structural refinements were performed using the BGMN/Profex 5.2.0 software.[2,3] Refined parameters included scale factors, background, peak shapes, crystallite size/microstrain broadening, lattice constants, preferred orientation effects, and isotropic thermal parameters. Structure .cif file for Cu_3VS_4 (ICSD-402891) from the Inorganic Crystal Structure Database (ICSD) was used for the refinement. Crystallite sizes were estimated by PDXL software using the Scherrer equation. Instrumental broadening was assessed with a standard reference sample and found to contribute less than 1% to the observed peak broadening, ensuring the reliability of the crystallite size estimation.

Yield Quantification. After drying under flowing N_2 overnight, Cu_3VS_4 nanocrystal powder from a 180 °C reaction temperature was weighed on an analytical balance, yielding a total mass of m_0 = 177.3 mg. The mass fractions of Cu_3VS_4 nanocrystals and surface ligands in as-synthesized nanocrystal powder were quantified with thermogravimetric analysis (TGA). A portion of the powder was heated to 500 °C under a N_2 atmosphere to volatilize the surface ligands, leaving only uncapped nanocrystals (Fig. S3). The phase and composition were confirmed to be Cu_3VS_4 by

powder XRD and SEM-EDX (Table S1). The mass fraction of nanocrystals in the as-synthesized powder can be calculated as

$$\omega = \frac{m_\mathrm{f}}{m_\mathrm{i}} \quad \textbf{(S1)}$$

where m_f is the final mass after ligand removal, and m_i is the initial mass. Thus, the total mass of ligand-free Cu_3VS_4 in the as-synthesized powder would be

$$m = m_0\omega \quad \textbf{(S2)}$$

where m_0 is the total mass of dry nanocrystal powder. The reaction yield can be calculated as

$$\eta = \frac{m}{Mn} \quad \textbf{(S3)}$$

where M = 369.8 g/mol is the molar mass of Cu_3VS_4, and n = 0.200 mmol is the amount of $VO(acac)_2$, the limiting reagent, in each reaction. Combining **eq S1–S3**,

$$\eta = \frac{m_0 m_\mathrm{f}}{Mnm_\mathrm{i}} = \frac{177.3\ \mathrm{mg} \times 33.5\ \mathrm{mg}}{369.8\ \mathrm{mg/mmol} \times 0.200\ \mathrm{mmol} \times 83.1\ \mathrm{mg}} = 96.6\% \quad \textbf{(S4)}$$

Considering minor product loss in the purification process, the reaction yield should be close to unity.

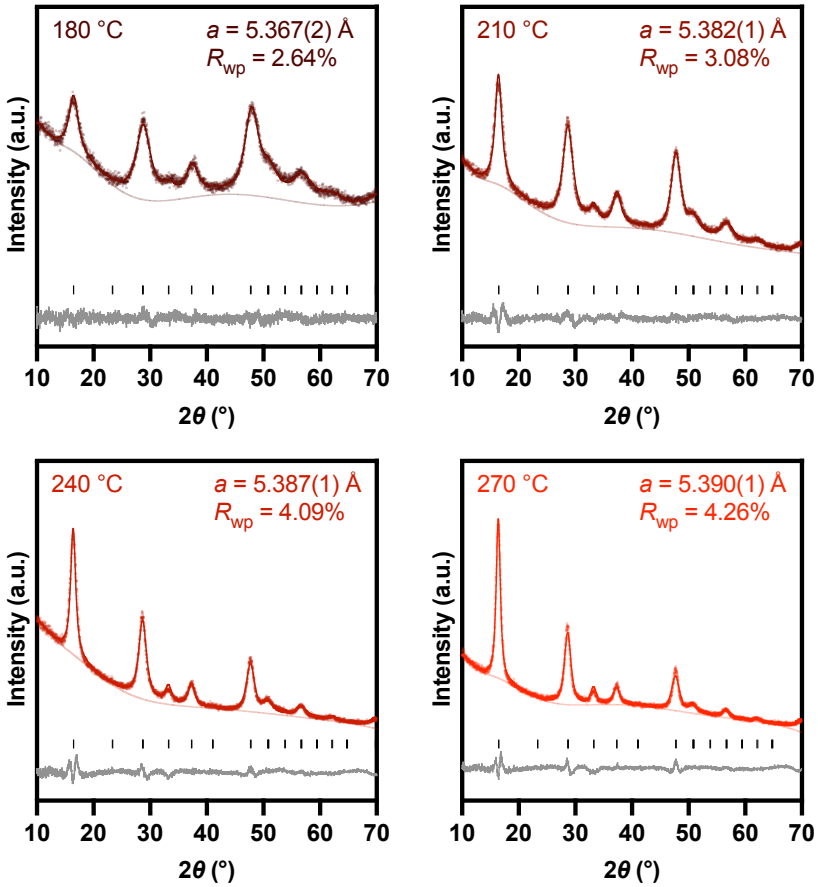

Fig. S1 Rietveld refinements of the laboratory powder XRD patterns of ultrasmall Cu_3VS_4 nanocrystals synthesized at various temperatures, with λ = 1.541 Å. All refined lattice parameters are in close agreement with the literature value, a = 5.393(1) Å for Cu_3VS_4 (ICSD-402891).

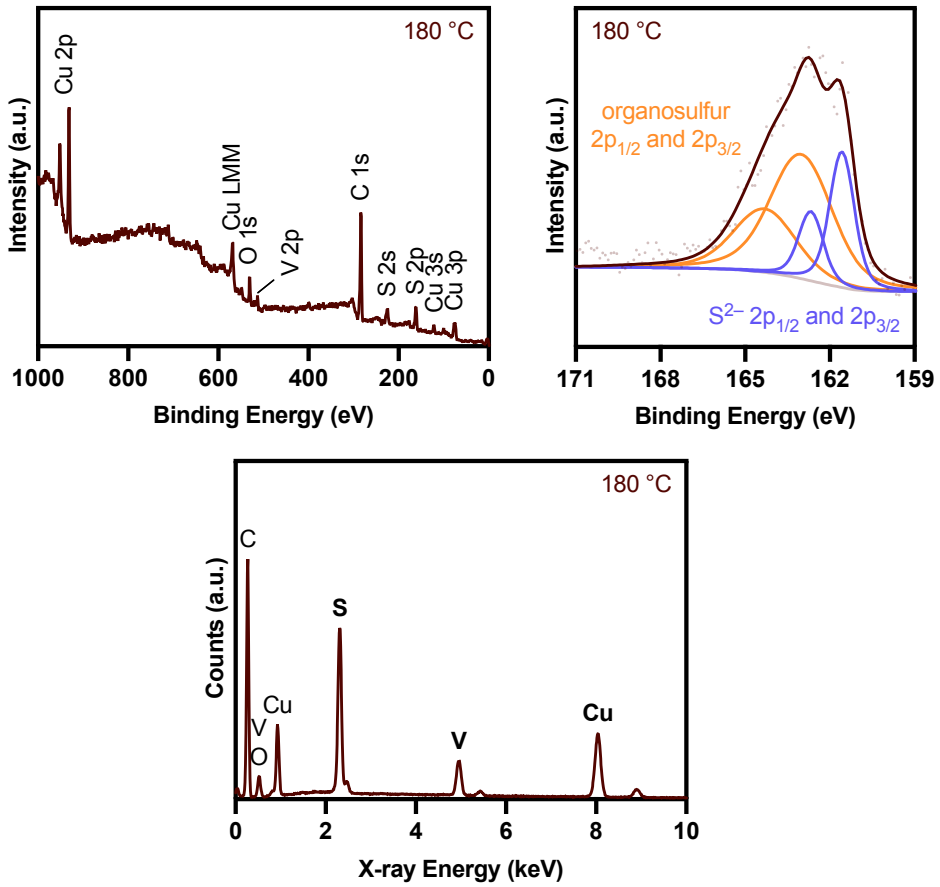

Fig. S2 XPS survey spectrum, high-resolution S 2p spectrum, and SEM-EDX spectrum of Cu_3VS_4 nanocrystals synthesized at 180 °C. The *K* line series for EDX semiquantitative analysis is highlighted in bold.

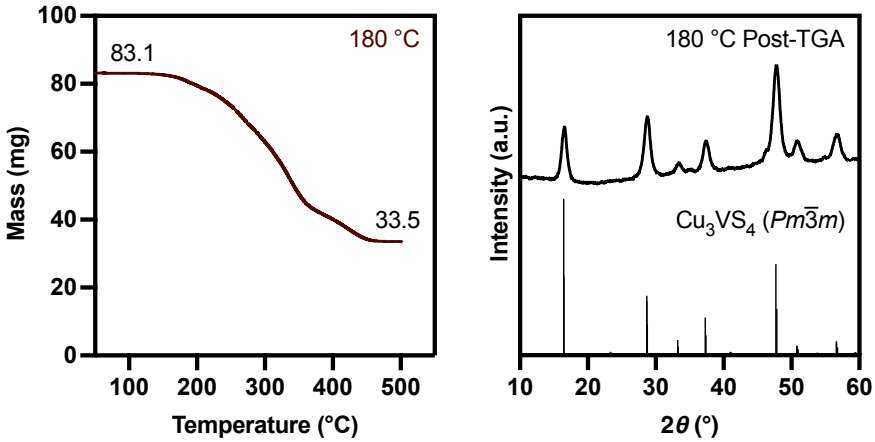

Fig. S3 TGA curve of dried Cu_3VS_4 nanocrystal powder synthesized at 180 °C and XRD pattern of the annealed powder. The TGA program involved heating to 500 °C at 10 °C/min and isotherm for 10 min. The isotherm period resulted in negligible mass loss (<0.1%), demonstrating complete removal of organic ligands. The Scherrer crystallite sizes of the annealed powder were τ_{100} = 8.7 nm and τ_{111} = 8.1 nm, indicating only mild sintering of nanograins.

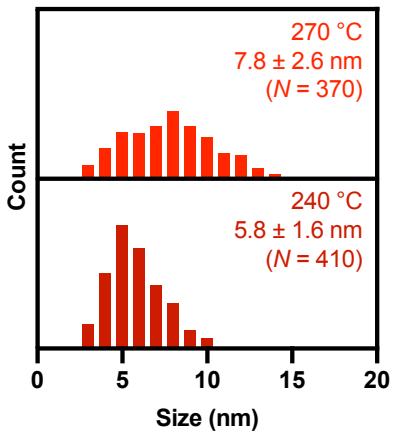

Fig. S4 Histograms showing the size (edge length) distributions of Cu_3VS_4 nanocrystals synthesized at 240 and 270 °C.

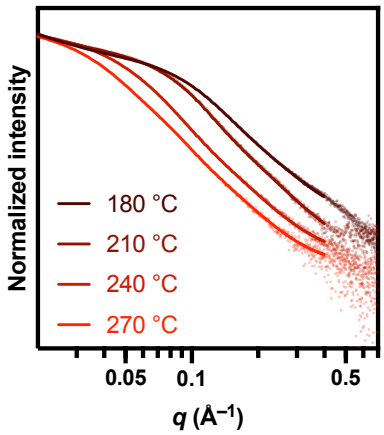

Fig. S5 SAXS patterns (circles) and corresponding fits (lines) for Cu_3VS_4 nanocrystals. The data were fit over a q-range of 0.02–0.4 $Å^{-1}$.

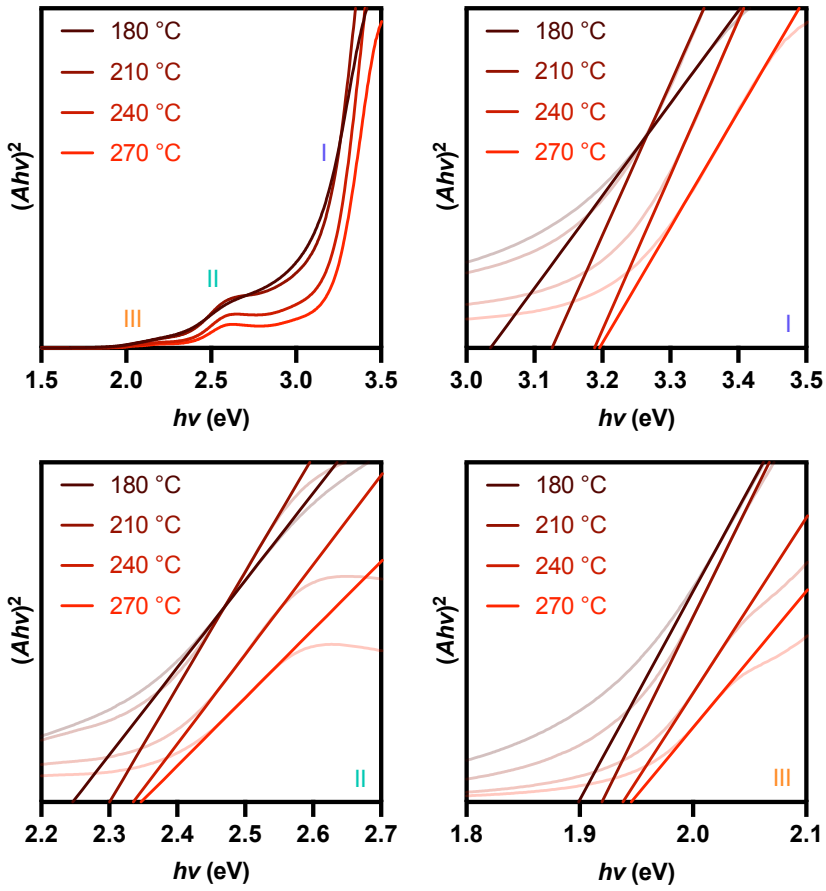

Fig. S6 Tauc plots of ultrasmall Cu_3VS_4 nanocrystals assuming direct allowed transitions and zoomed-in linear fits of each feature for the determination of absorption energy.

s

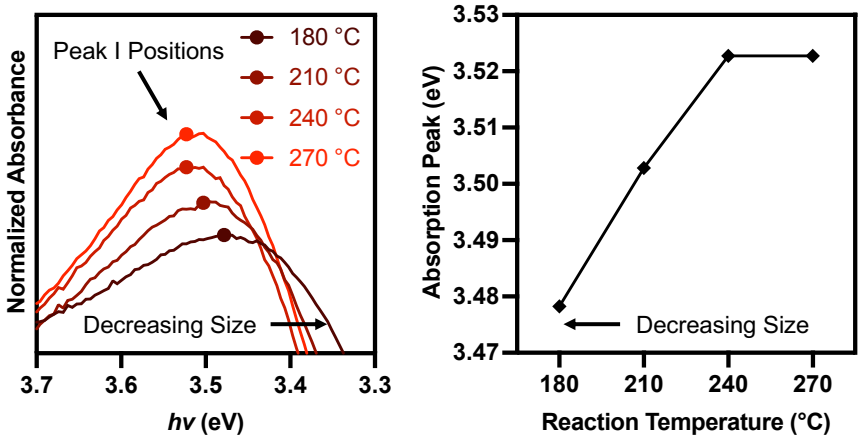

Fig. S7 Zoomed-in view of feature I in the UV-vis-NIR absorbance spectra (Fig. 4a) and corresponding absorption peak energies, showing gradual redshifts with decreasing nanocrystal size.

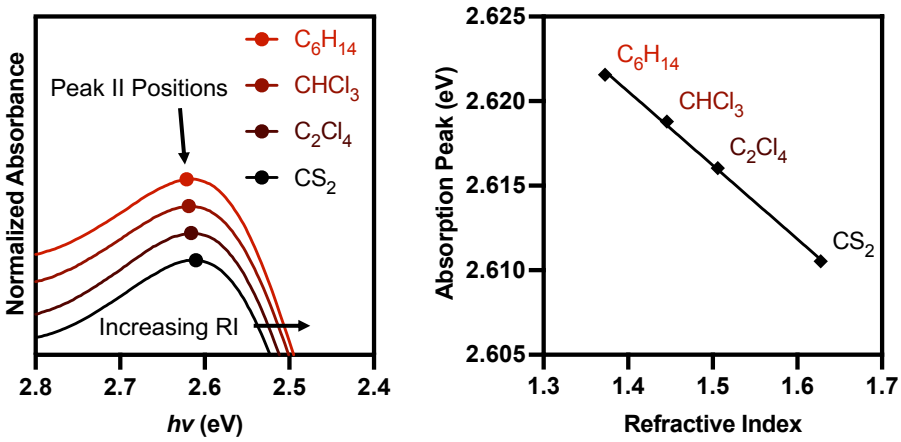

Fig. S8 Zoomed-in view of feature II in the UV-vis-NIR absorption spectra of Cu_3VS_4 nanocrystals synthesized at 240 °C (~6 nm) and dispersed in various solvents: hexanes (C_6H_{14}), chloroform ($CHCl_3$), tetrachloroethylene (C_2Cl_4), and carbon disulfide (CS_2). Feature II was analyzed due to the overlap of feature I with the intrinsic absorption of CS_2. The extracted peak energy decreases linearly with increasing solvent refractive index, consistent with the behavior previously reported for 12 nm Cu_3VS_4 nanocrystals.[4]

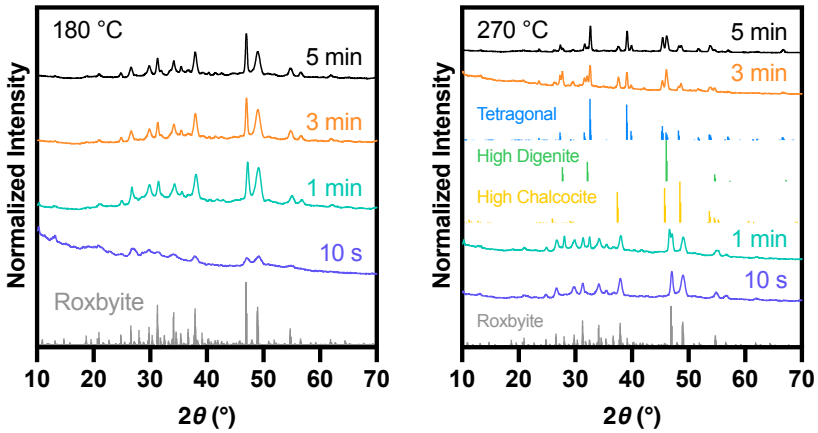

Fig. S9 Powder XRD patterns of reaction aliquots collected from syntheses performed without the $VO(acac)_2$ precursor, compared with stick patterns of $Cu_{2-x}S$ phases, including roxbyite ($P\bar{1}$, ICSD-185807), tetragonal ($P4_32_12$, ICSD-185807), high digenite ($Fm\bar{3}m$, ICSD-53330), and high chalcocite ($P6_3/mmc$, ICSD-53329). At 180 °C, roxbyite $Cu_{2-x}S$ nucleated upon injection and persisted throughout the reaction. At 270 °C, roxbyite $Cu_{2-x}S$ initially nucleated and subsequently transformed into a mixture of tetragonal, high digenite, and high chalcocite phases upon prolonged heating.

Table S1 Elemental compositions of nanocrystal samples acquired by SEM-EDX. All atomic percentages exceeded three times their respective errors, ensuring statistical significance.

Sample	Cu at%	V at%	S at%	V/Cu ratio	S/Cu ratio
Ideal Cu_3VS_4 stoichiometry	37.5	12.5	50	0.33	1.33
Cu_3VS_4 nanocrystals					
180 °C	29.91(11)	10.67(9)	59.42(20)	0.36	1.99
210 °C	32.65(8)	11.39(6)	55.96(15)	0.35	1.71
240 °C	33.24(8)	11.81(6)	54.94(15)	0.36	1.65
270 °C	32.88(8)	11.92(6)	55.20(15)	0.36	1.68
180 °C, post-TGA	37.79(9)	12.83(8)	49.38(16)	0.34	1.31
180 °C, aliquot study					
10 s	32.66(10)	7.65(6)	59.68(18)	0.23	1.83
1 min	49.52(9)	5.74(5)	44.74(18)	0.12	0.90
3 min	35.05(9)	8.42(6)	56.53(18)	0.24	1.61
270 °C, aliquot study					
10 s	55.17(9)	3.75(5)	41.08(19)	0.07	0.74
1 min	39.03(9)	11.00(6)	49.97(19)	0.28	1.28
3 min	38.13(9)	10.74(6)	51.13(19)	0.28	1.34

References

1 M. Doucet, M. Adams, N. Agouzal, G. Alina, A. Anuchitanukul, Z. Attala, J. Bakker, P. Beaucage, J. Berger, R. Bourne, W. Bouwman, I. Bressler, P. Butler, I. Cadwallader-Jones, K. Campbell, J.-H. Cho, T. Cooper-Benun, R. Cortes Hernandez, J. Doutch, D. Dresen, G. Drosos, C. Durniak, C. Farrow, R. Ferraz Leal, R. Ford, L. Forster, J. Gaudet, M. Gerina, P. Gilbert, M. Gonzalez, O. Hammond, R. Heenan, S. Henson, E. Hewins, D. Honecker, A. Jackson, G. Jensen, P. Juhas, J. Karliczek, P. Kienzle, S. King, S. Kline, J. Krzywon, S. B. Lee, J. Lin, Y. Liu, R. Lopes, D. Lozano, K. Lytje, D. Mannicke, B. Maranville, A. Markvardsen, N. Martinez, M. McKerns, B. Miller, K. Mothander, R. Murphy, A. Nelson, T. Nielsen, M. Oakley, L. O'Driscoll, H. Park, P. Parker, M. Patrou, P. Peterson, W. Potrzebowski, S. Prescott, M. Rakitin, T. Richter, J. Rooks, P. Rozyczko, X. Shan, T. Snow, A. Stellhorn, S. Teixeira, J. Tumarkin, A. Washington, K. Weigandt, R. Whitley, L. Wilkins, C. Wolf, A. Zhang, A. Zheng, G. Fragneto, B. Fultz, T. Perring, T. H. Rod and J. Taylor, SasView version 6.0.1 (version 6.0.1) Zenodo 2025.

2 N. Doebelin and R. Kleeberg, *J. Appl. Crystallogr.*, 2015, **48**, 1573–1580.

3 R. A. Young, Ed., *The Rietveld Method*, Oxford University Press, Oxford, 1993.

4 Y. Liu, T. Ding, X. Luo, Y. Li, J. Long and K. Wu, *Chem. Mater.*, 2020, **32**, 224–233.